Persistence of cluster synchronization under the influence of advection

Emma Guirey,[1,*,†] Martin Bees,[2] Adrian Martin,[1,†] and Meric Srokosz[1,†]
[1]*National Oceanography Centre, Southampton SO14 3ZH, United Kingdom*
[2]*Department of Mathematics, University Gardens, University of Glasgow, Glasgow G12 8QW, United Kingdom*
(Received 3 November 2009; revised manuscript received 1 February 2010; published 3 May 2010)

We present a study on the emergence of spatial structure in plankton dynamics under the influence of stirring and mixing. A distribution of plankton is represented as a lattice of nonidentical, interacting, oscillatory plankton populations. Each population evolves according to (i) the internal biological dynamics represented by an NPZ model with population-specific phytoplankton growth rate, (ii) sub-grid-cell stirring and mixing parameterized by a nearest-neighbor coupling, and (iii) explicit advection resulting from a constant horizontal shear. Using the methods of synchronization theory, the emergent spatial structure of the simulation is investigated as a function of the coupling strength and rate of advection. Previous work using similar methods has neglected the effects of explicit stirring (i.e., at scales larger than the grid cell), leaving as an open question the relevance of the work to real marine systems. Here, we show that persistent spatial structure emerges for a range of coupling strengths for all realistic levels of surface ocean shear. Spatially, this corresponds to the formation of temporally evolving clusters of local synchronization. Increasing shear alters the spatial characteristics of this clustering by stretching and narrowing patches of synchronized dynamics. These patches are not stretched into stripes of synchronized abundance aligned with the flow, as may be expected, but instead lie at an angle to the flow. This study shows that advection does not diminish the relevance of conclusions from previous studies of spatial structure in plankton simulations. In fact, the inclusion of advection adds characteristic filamental structure, as observed in real-world plankton distributions. The results also show that the ability of coupled oscillators to synchronize depends strongly on the spatial arrangement of oscillator natural frequencies; under the influence of advection, therefore, the impact of the coupling strength on the emergent spatial structure of a biophysical simulation is time-dependent.

DOI: 10.1103/PhysRevE.81.051902 PACS number(s): 87.18.Hf, 87.23.Cc

I. INTRODUCTION

There has, in the scientific literature, been extensive and continued interest in the use of synchronization theory to study spatiotemporal fluctuations in natural populations. Synchronization theory is concerned with how the natural rhythms of time-varying entities adjust as a result of interaction between them [1] and finds examples across all areas of science from electronics (e.g., [2,3]) and lasers (e.g., [4]) to epidemiology (e.g., [5]), fireflies [6] and the human body (e.g., [7,8]). Spatially synchronized fluctuations in natural populations have been documented for a wide variety of species including rodents [9–11], birds [12], fish [12], mammals [11,13], insects [14], and plankton [15]. This has lead Ranta *et al.* [12] to claim that studying spatial synchrony, where previously the focus has been on temporal fluctuations of individual populations, should help ecologists get to the core of the workings of population dynamics.

Ecologists have applied synchronization theory to a variety of, mainly terrestrial, ecosystems by modeling a region of interest as a metapopulation of discrete populations interacting directly or indirectly via, for example, common environmental forcing, a common predator or migration between populations (e.g., [9,10,13,16]). Researchers have applied similar methods in a marine context, looking at the spatial structure arising in distributions of surface ocean plankton [15,17–20]. The motivation for studying spatial and temporal heterogeneity, or "patchiness," in plankton comes from their key role in the carbon cycle, their significance as the base of most marine foodwebs and the inherent interest in how microscopic apparently "free floating" organisms can form and maintain spatial structure under the homogenizing influence of ocean stirring and mixing. Empirical studies [21] have shown that a patchy plankton distribution has a lower risk of extinction than a homogeneous one because asynchronously varying populations allow recolonization of depleted patches. It is, therefore, important to understand the conditions under which nearby populations might vary synchronously.

Initial modeling studies represented a spatial distribution of plankton as a one-dimensional chain of identical plankton populations with nearest-neighbor interaction [17,19]. The key result from these studies is that a critical strength of coupling between populations exists, with system-level dynamics altering from asynchronous (heterogeneous), for coupling weaker than the critical value, to fully synchronized (homogeneous; all populations evolve identically in time) for stronger coupling. Furthermore, the critical coupling was found to depend upon the size of the system, the spatial resolution, the biological model representing plankton dynamics of each population and the biological model parameters. The worrying consequence of this work for biophysical modeling is that potentially arbitrary choices of standard simulation parameters can determine whether patchy or homogenous system-level dynamics occur.

*Corresponding author; e.j.guirey@marlab.ac.uk
†Present address: Marine Laboratory, Marine Scotland, P.O. Box 101, 375 Victoria Road, Aberdeen AB10 9DB, UK.

Further work incorporated spatial variability by looking at interacting nonidentical populations; the biological model parameters describing the dynamics of each population were allowed to vary in space [18,20]. It was shown that coupling between populations could induce phase synchronization, with populations frequency-locked (i.e., all populations fluctuate with the same frequency) and in-phase but with varying amplitudes. This is a phenomenon widely documented in natural spatial population dynamics [11,22].

Subsequent work [20] increased the realism and oceanographic relevance of this approach by simulating a distribution of surface ocean plankton as a two-dimensional lattice of nonidentical oscillatory populations. The populations interacted via a nearest-neighbor parameterization of sub-grid-cell mixing and stirring. Recognizing that this setup, although simplified, is directly analogous to the standard approach to biophysical simulation of the surface ocean, Guirey *et al.* [20] explored the emergence of spatial structure in biophysical simulations as a function of underlying physical model structure. It was found that the emergent spatial structure depends in a discontinuous manner on the strength of interaction between populations. A critical value of coupling was found above which the populations became frequency locked. Surprisingly, however, the relationship between strength of interaction and degree of synchrony between populations was not monotonic. Instead, intermediate coupling strengths less than the critical value for frequency locking were found that induced a tenfold *increase* in the spatial variability between populations over the uncoupled level. This "anomalous route to synchrony" has been described by Blasius and Montbrió [16] for coupled oscillatory predator-prey systems. Guirey *et al.* [20] reported that the anomalous coupling range of apparent desynchronization manifested spatially as clustering of populations into persistent, irregularly shaped and constantly evolving and shifting patches of local synchrony. This phenomenon is known as cluster synchronization [23–26]. Within the frequency-locked regions of coupling strength, the spatiotemporal dynamics consisted of quasiregular traveling waves of phase synchronization. This effect has been observed by Blasius *et al.* [27] and Blasius and Tönjes [28] for a two-dimensional simulation of coupled nonidentical predator-prey populations and has been reported for natural populations (e.g., [9]).

A key criticism that can be leveled at previous work, from a marine perspective, is that the only representation of the effects of the flow of water is the sub-grid-cell stirring and mixing, parameterized as an effective diffusivity. Whilst all ocean simulations have to take account of the sub-grid-cell flow processes, they will in general also have an explicit representation of stirring at larger scales. Critics could argue that the inclusion of these processes will destroy the spatial structure due to synchronization effects seen in previous studies, thereby rendering the results irrelevant. Therefore, it is important to address the question: will spatial structure related to synchronization effects persist under the influence of explicit stirring? This is related to the question of how plankton retain coherent structure under the homogenizing influence of stirring and mixing in the real world (see, e.g., [29]).

To address these valid criticisms, we apply to the framework used by Guirey *et al.* [20] a simple shear flow resulting in differential horizontal advection at scales larger than the grid cell, and explore the impact of the rate of this flow on the emergent spatial properties of a surface ocean plankton simulation. The scheme is chosen as the simplest possible flow such that water masses can move at different speeds relative to one another; it provides an ideal basis to begin studying the influence of advection on interacting populations. This has not been studied previously, largely because most studies of synchronization phenomena in metapopulations have been carried out in a terrestrial context, with which the present study is not directly analogous. This study addresses the question of whether synchronization-related spatial clustering occurs under the influence of explicit advection and how the flow affects the ability of a coupled system of plankton populations to synchronize.

In particular, we model the distribution of plankton in a surface ocean region as a two-dimensional lattice of oscillatory populations, the biological dynamics of each represented by a typical Nutrient-Phytoplankton-Zooplankton model. Parameter mismatch is applied to the biological parameters of the populations to give small variation in the frequency and amplitude of oscillation in the absence of interaction, which we refer to as the "natural" properties of the populations. The populations interact through a nearest neighbor coupling parameterizing sub-grid-cell stirring and mixing. A constant horizontal shear is applied to the lattice in one dimension, resulting in advection of populations with respect to one another. The degree of synchrony between populations and the emergent spatial structure of the simulation is a function of both the nearest neighbor coupling strength and the rate of shear, which are varied within realistic oceanic ranges.

This study will address the issue of whether the results and methods of synchronization theory from terrestrial metapopulation dynamics and the previous studies on plankton patchiness are relevant in a marine context. Additionally, it will show whether the worrying abrupt changes in system-level dynamics observed in previous simulations remain a concern for more realistic scenarios. The increase in realism will also help to show the way forward in developing these methods for studying real-world plankton distributions.

II. METHODS

A. Model

We represent the distribution of plankton in a spatially varying surface ocean region of size L km $\times L$ km as a two-dimensional lattice of $n \times n$ populations. Each population evolves according to (i) the internal biological dynamics represented by the same Nutrient-Phytoplankton-Zooplankton model but with population-specific parameters, (ii) sub-grid-cell-scale stirring and mixing processes parameterized by a nearest neighbor coupling term and (iii) an explicit advection term resulting from a constant horizontal shear. This model, without (iii), is exactly that used by Guirey *et al.* [20] to study the dependence of emergent spatial structure in plankton simulations on the strength of interaction between populations [i.e., (ii)]. The essential details are summarized here. See Guirey *et al.* [20] for more information.

The biological dynamics of each population is represented by the Nutrient-Phytoplankton-Zooplankton (NPZ) model originally formulated by Steele and Henderson [30],

$$\frac{dN}{dt} = -\frac{a_0 N}{(e+N)(b+cP)}P + rP + \frac{\zeta\beta P^2}{\mu^2+P^2}Z + \gamma dZ + k(N_0 - N)$$
$$= -\text{uptake} + \text{respiration} + Z \text{ excretion} + Z \text{ predators excretion} + \text{mixing}, \quad (1)$$

$$\frac{dP}{dt} = \frac{a_0 N}{(e+N)(b+cP)}P - rP - \frac{\zeta P^2}{\mu^2+P^2}Z - sP - kP$$
$$= \text{uptake} - \text{respiration} - \text{grazing by } Z - \text{sinking} - \text{mixing}, \quad (2)$$

$$\frac{dZ}{dt} = \frac{\zeta\alpha P^2}{\mu^2+P^2}Z - dZ$$
$$= \text{growth due to grazing on } P - \text{higher predation}. \quad (3)$$

Briefly, this is a zero-dimensional model representing the processes occurring in a physically homogeneous region of upper ocean mixed layer, with mixed layer depth and irradiance assumed constant. Phytoplankton, P, zooplankton, Z, and nutrient, N, concentrations are explicitly represented. An implicit biologically inactive deeper layer with a fixed nutrient content acts by way of vertical mixing as a nutrient source for the upper layer biology. The change in phytoplankton concentration is modeled as the sum of growth, colimited by nutrients and light (represented as a self-shading term), and losses due to respiration, mixing and sinking out of the upper layer, and grazing by zooplankton. Of the material grazed by zooplankton, a constant fraction is assimilated, contributing to zooplankton growth. A parameterization of predation by higher predators closes the food chain from above. A fixed proportion of the material grazed by zooplankton and higher predators is excreted back to the nutrient pool. The zooplankton is assumed to possess enough mobility to remain within the mixed layer.

Exploration of the dynamics of this model for an individual population can be found in work by Guirey *et al.* [19], Steele and Henderson [30], Edwards and Brindley [31,32]. Here, we use a default biological model parameter set (Table I) for which the model exhibits regular oscillatory behavior. This is the simplest time-varying behavior not due to any external forcing, which is neglected to avoid introducing an additional time scale of variation. This study is intended to be illustrative; we do not attempt to accurately reproduce the plankton dynamics of any particular time and place but instead focus on exploring the underlying dynamics and mechanisms of pattern formation.

To incorporate the spatial variability inherent in nature, the parameter set best describing the dynamics of each subpopulation is assumed to vary: a small mismatch is added to the default phytoplankton growth rate a_0 for each population. Such variability could arise, for example, from spatial variation in temperature [33] or mixed layer depth [34]. The phytoplankton growth rates are chosen from a uniform distribution of width Δ centered on a_0, so that $a_{i,j} \in [a_0 - \frac{\Delta}{2}, a_0 + \frac{\Delta}{2}]$ for $i,j = 1,\ldots,n$.

TABLE I. Default biological model parameters. Population-specific phytoplankton growth rates $a_{i,j}$, for $i,j=1,\ldots,n$, are selected from a uniform distribution of width 5% of a_0 centered on a_0.

Parameter	Symbol	Value	Units
P growth parameter	a_0	0.2	m^{-1} $days^{-1}$
Light attenuation by water	b	0.2	m^{-1}
Self-shading by P	c	0.4	m^2 gC^{-1}
Herbivorous Z mortality	d	0.14	$days^{-1}$
N half-saturation constant	e	0.03	gC m^{-3}
Exchange rate with lower layer	k	0.05	$days^{-1}$
P respiration	r	0.15	$days^{-1}$
P sinking	s	0.04	$days^{-1}$
Lower layer N concentration	N_0	1.0	gC m^{-3}
Herbivorous Z assimilation efficiency	α	0.25	
Z excretion fraction	β	0.33	
Remineralization of Z excretion	γ	0.5	
Herbivorous Z grazing rate	ζ	0.6	$days^{-1}$
Herbivorous Z grazing half-sat. const.	μ	0.035	gC m^{-3}

Stirring and mixing between populations at sub-grid-cell scales is parameterized by a nearest neighbor coupling term. In the usual case of no explicit advection, this may be formulated as

$$\dot{v}_{i,j} = F_{i,j}(v_{i,j}) + \varepsilon \cdot (v_{i-1,j} + v_{i+1,j} - 4v_{i,j} + v_{i,j-1} + v_{i,j+1}),$$

where $v_{i,j} = (N_{i,j}, P_{i,j}, Z_{i,j})$, the function $F_{i,j}$ is the NPZ model described above with population-specific phytoplankton growth rate $a_{i,j}$ and ε is the strength of interaction between populations in $days^{-1}$.

The coupling term represents mixing processes between adjacent grid-cells so that

$$\varepsilon \cdot (v_{i-1,j} + v_{i+1,j} - 4v_{i,j} + v_{i,j-1} + v_{i,j+1}) \approx D\frac{\partial^2 v_{i,j}}{\partial x^2},$$

where D is the effective diffusivity between grid cells. Hence we may equate ε with the effective diffusivity so that $\varepsilon \approx Dl^{-2}$ where $l = \frac{L}{n}$ is the grid-cell length scale and $\frac{1}{l^2}$ approximates the second order spatial derivative. The effective diffusivity has been shown by Okubo [35] to scale with length scale according to the empirical relationship $D(l_s) \approx 0.01 l_s^{1.15}$ with l_s in cm and effective diffusivity $D(l_s)$ in cm^2 s^{-1}. If we take the grid-cell length scale l of the lattice as the spatial scale at which effective diffusivity acts in the model, then $\varepsilon \approx 0.01 l^{-0.85} \times 60 \times 60 \times 24$ for ε in $days^{-1}$. For mesoscale processes on the order of 1 km to 100 km, this gives a range of coupling $\varepsilon \in [0.001, 0.05]$ $days^{-1}$ between adjacent grid cells with coupling strength increasing with decreasing length scale. Since an understanding of the uncoupled system ($\varepsilon = 0$) is essential to an understanding of the coupled system ($\varepsilon > 0$), we consider the range

$\varepsilon \in 0 \cup [0.001, 0.05]$ days^{-1}. Varying ε in this range is equivalent to varying the spatial resolution of the model from 100 km to 1 km, i.e., $l \in [1, 100]$ km, and the domain size L therefore also varies with ε. It is possible instead to vary n with ε so that L is fixed. However, the ability of coupled populations to synchronize their dynamics varies with the number of populations (e.g., [1,19,36]), so here n is fixed to allow for a clearer analysis.

Here, we introduce explicit advection into the simulation, resulting from constant shear

$$\frac{\partial u}{\partial y} = -\Gamma,$$

(where the positive y axis is defined as distance from the top edge of the lattice and Γ is in days^{-1}) so that the water speed u in the x direction varies linearly with y.

In the spatially discrete model, this means that row i advects at a speed $\Gamma \cdot l$ km days^{-1} with respect to row $i+1$. Boundary conditions are singly periodic, allowing advected material leaving the domain at $x=0$ to re-enter at $x=L$; no-flux boundary conditions are imposed at $y=0$ and $y=L$. Previous work [20] found no sensitivity to the choice of boundary conditions and singly periodic boundary conditions are the natural choice under the flow scheme imposed here. The implementation of this shear requires that rows of the lattice travel at different speeds and, therefore, the grid cells become misaligned in the y direction. At each time-step of δt days, row i is shifted with respect to row $i+1$ by a distance $\rho \cdot l$ where $\rho \in [0, 1)$. The fraction ρ of a grid cell moved at each time step is determined by the rate of shear, such that

$$\Gamma = \frac{\partial u}{\partial y} = \frac{\rho l / \delta t}{l} = \frac{\rho}{\delta t},$$

and, therefore, $\rho = \Gamma \times \delta t$. Since the inclusion of shear causes rows to become misaligned, there is an additional nearest-neighbor interaction of population $v_{i,j}$ with populations $v_{i-1,j-1}$ and $v_{i+1,j+1}$ and the coupling term becomes a time-varying function,

$$\varepsilon[\{A(t)v_{i-1,j-1} + [1 - A(t)]v_{i-1,j} + v_{i,j-1} - 4v_{i,j} + v_{i,j+1} + [1 - A(t)]v_{i+1,j} + A(t)v_{i+1,j+1}\},$$

for rows $i = 1, \ldots, n$ and columns $j = 1, \ldots, n$, with

$$A(t) = \rho\left[\left(\frac{t}{\delta t}\right) \mathrm{mod}\left(\frac{1}{\rho}\right)\right],$$

so that $0 \leq A(t) < 1$. Every $\frac{1}{\rho}$ time steps, the rows are misaligned with one another by a whole grid cell, whereupon there is a reindexing of the populations to reflect the new position occupied in the lattice and accounting for the singly periodic boundary conditions. The populations are taken to advect with the parcels of water, so that a reindexing of the population-specific growth rates $a_{i,j}$ is also applied, resulting in a time-dependent arrangement of population growth rates and, therefore, natural (uncoupled) properties. This assumes that the spatial variability is related to local properties of the water or the populations themselves. The dynamics $v_{i,j}(t)$, therefore, represent an Eulerian time series describing the biological evolution of the area of ocean bounded by the lattice. Additionally, a Lagrangian time series is recorded describing the evolution of the biology in the parcel of water originally labeled (i,j) and subsequently occupying a time-varying position on the lattice. To clarify, if (I,J) and (i,j) denote a population's original position and time-varying position, respectively, on the lattice, then we have an Eulerian time series as described above: $v_{i,j}$ with $i = I \forall t$ and $j = g(I,J,t) = [J - \Gamma t] \mathrm{mod}(n)$, where $[x]$ denotes the largest integer less than or equal to x. Then we have a Lagrangian time series $v_{I,J}$, with

$$\dot{v}_{I,J} = F(I,J) + \varepsilon\{A(t)v_{I-1,J'-1} + [1 - A(t)]v_{I-1,J'} + v_{I,J-1} - 4v_{I,J} + v_{I,J+1} + [1 - A(t)]v_{I+1,J''} + A(t)v_{I+1,J''+1}\},$$

where $J' = g(I-1, J, t)$, $J'' = g(I+1, J, t)$, $A(t) = (J - \Gamma t) - [J - \Gamma t]$ and a_0 in $F_{I,J}$ is $a_{I,J} \forall t$.

B. Details of runs

We explore the impact of shear on the emergent spatial structure generated by interaction between populations. The parameter spread $\Delta = 5\%$ of a_0 so that $a_{i,j} \in [0.195, 0.205]$ days^{-1}. This choice of Δ is deliberately conservative to give a set of subpopulations with essentially the same dynamics but small variation in amplitude and period of oscillation. The resulting spread in natural frequencies is $\sim 2.5\%$. Without interaction between populations ($\varepsilon = 0$), a simulation run from initially homogenous conditions leads quickly to a random field.

Simulations are carried out for $\Gamma = 0.0$ days^{-1}, $\Gamma = 0.001$ days^{-1}, $\Gamma = 0.005$ days^{-1}, $\Gamma = 0.01$ days^{-1}, $\Gamma = 0.05$ days^{-1}, and $\Gamma = 0.1$ days^{-1}, covering a range typical of surface ocean shear [37,38]. For each value of shear, the coupling strength ε is varied in the range given above. As explained, the emergent dynamics of the lattice are determined by the influences of the biological dynamics, the effective diffusivity and the advection caused by shear, each of which has an associated time scale: T_{NPZ}, T_ε, and T_Γ, respectively. $T_{\mathrm{NPZ}} \approx 100$ days is the period of oscillation of the populations. $T_\varepsilon = \frac{1}{\varepsilon}$ ranges from 20 to 1000 days since $\varepsilon \in [0.001, 0.05]$ days^{-1}. Hence the values of Γ give advection time scales $T_\Gamma \in [10, 1000]$, covering a range slower than, equal to and faster than T_{NPZ} and T_ε. Note that this study is intended to be illustrative; no attempt has been made to reproduce seasonal plankton dynamics and T_{NPZ} has not been tuned to any particular time scale. It is expected that the results will remain qualitatively unchanged unless T_{NPZ} is faster than 10 days, the fastest time scale associated with the shear, Γ. The case $\varepsilon = 0$ days^{-1} is included for completeness. ε and Γ are held constant throughout each simulation, which is run from initially homogenous conditions until transient dynamics die away. For a detailed description of the transient dynamics see Guirey *et al.* [20]. The length of transient was found to vary with ε so that, especially near to bifurcations in system behavior (see below), an integration of up to 5000 days was required. Results for zero shear were not found to be sensitive to the choice of initial conditions; results for nonzero shear are time varying and therefore do depend on initial conditions, as will be seen below.

Since this advection scheme results in a time-varying arrangement of phytoplankton growth rates and, therefore, population natural properties, some additional simulations were carried out to highlight the impact of the spatial arrangement of population properties on the synchronization effects exhibited by the system. Every $\frac{1}{\rho}$ time steps, the populations in each row have shifted by a whole grid cell with respect to neighboring rows. Because of the differential rate of horizontal flow, it takes $n \times \frac{1}{\rho}$ time steps before all populations return to their original position on the lattice. Hence, n different configurations with grid-cells aligned result from the shear flow: $a_0(m)=A_{I,J+mI}$, where $m=0,1,\ldots,n-1$ and $A_{I,J}$ is the configuration under zero shear. For ease of performing ensemble runs, a 10×10 lattice of populations was chosen, with all other parameters as above. For shear rates $\Gamma=0$ days^{-1}, $\Gamma=0.001$ days^{-1}, and $\Gamma=0.1$ days^{-1}, simulations were carried out for the full range of coupling strength ε for each of the ten possible advection-induced initial spatial arrangements of the natural frequencies.

C. Diagnostics

The resultant behavior of the simulation for varying ε and Γ is characterized using several metrics.

(1) Two-dimensional phytoplankton biomass field, $P_{i,j}$. A visual indication of the spatial dynamics is obtained from the two-dimensional Eulerian fields of phytoplankton, zooplankton, and nutrient concentration. For brevity, results are presented for phytoplankton dynamics only; similar synchronous properties are observed for zooplankton and nutrient dynamics.

(2) Frequency spread, σ. The time average angular frequency $\omega_{i,j}$ of each subpopulation is calculated by using the Lagrangian time series, for 500 days after steady state dynamics have been reached, to obtain a time series $T_{i,j}$ of peak abundance in one of the state variables, $N_{i,j}$, $P_{i,j}$, or $Z_{i,j}$. Then

$$\omega_{i,j} = \left(\frac{n-1}{T_{i,j}(n) - T_{i,j}(1)} \right) \times 2\pi,$$

where there are n peaks in the series. From the set of frequencies, the spread is

$$\sigma = \frac{\text{s.d.}(\omega_{i,j})}{\text{mean}(\omega_{i,j})} \times 100,$$

where s.d. denotes standard deviation and $\text{mean}(\omega_{i,j}) = \frac{1}{n^2}\Sigma_{i=1}^{n}\Sigma_{j=1}^{n}\omega_{i,j}$. The populations are said to be *frequency locked* when $\sigma=0$.

(3) Phase order, R. By linearly interpolating between peaks, the phase of oscillation of each population at a time t is approximated by

$$\theta_{i,j}(t) = \left(\frac{t - T_{i,j}(m-1)}{T_{i,j}(m) - T_{i,j}(m-1)} \right) 2\pi,$$

where $T(m)$ is the first peak occurring after time t. The centroid of the oscillators positions on the circle is then

$$Z = Re^{\iota\psi} = \frac{1}{n^2}\sum_{i=1}^{n}\sum_{j=1}^{n} e^{\iota\theta_{i,j}},$$

so that ψ gives the average phase and the order parameter R is a measure of the phase coherence of the populations. For uncorrelated phases, R is around 0. For populations oscillating with a common phase, $R=1$ and the system is said to be *phase synchronized*. Intermediate values of R indicate that the phases of the populations are neither equal nor randomly spread, e.g., local synchrony or *clustering*.

(4) Cluster measures, c_x and c_y. While σ and R measure the coherency in behavior of the ensemble as a whole, they can mask local synchronous effects such as clustering of the lattice into synchronized subsets of populations. Hence, we use a simple *cluster measure* $c \in [1,n]$ in numbers of grid cells that gives an indication of the size of spatial structure in one dimension. For zero coupling, $c=1$ because populations oscillate in isolation and no spatial structure exists larger than the grid cell. For a fully (phase and frequency) synchronized system, $c=n$. A value of c between 1 and n indicates some degree of local synchronization. The size of structure is examined in the x and y directions separately to obtain c_x and c_y. c_x is calculated by taking the $n\times n$ $P_{i,j}$ field

$$\mathbf{P}(t) = \begin{pmatrix} P_{11} & P_{12} & \cdots & P_{1n} \\ P_{21} & \cdots & \cdots & P_{1n} \\ \vdots & & & \\ P_{n1} & P_{n2} & \cdots & P_{nn} \end{pmatrix}$$

and removing its mean to obtain $\bar{\mathbf{P}}(t)=\mathbf{P}(t)-\frac{1}{n^2}\Sigma_{i=1}^{n}\Sigma_{j=1}^{n}P_{i,j}$. A transect $P_i=(\bar{P}_{i1},\bar{P}_{i2},\ldots,\bar{P}_{in})$ is taken across the lattice for each of the $i=1,\ldots,n$ rows of grid cells of the mean-removed field. A cluster is defined as a region of adjacent grid cells with continuously positive or negative values and is calculated by recording zero-crossings of P_i. Over all rows, this gives a set of clusters $\mathrm{C}_x=\{c_1,c_2,\ldots,c_m\}$, where c_k, for $k=1,\ldots,m$, are integer numbers of grid-cells and $\Sigma_{k=1}^{m}(c_k)=n^2$. The median of this set of clusters is then calculated for each time step to give a measure of the local coherency $c_x(t)$. The median, rather than mean, value is selected to prevent errors arising from clusters that straddle the $x=0$ and $x=L$ boundaries as a result of the periodic boundary conditions. $c_y(t)$ is calculated in exactly the same manner, but using columns rather than rows of $\bar{\mathbf{P}}(t)$.

These measures, summarized in Table II, are used together to enable a full description of how the emergent spatial structure of the plankton distribution, as a function of the strength of interaction between populations, is modified by the inclusion of advection.

III. RESULTS

A. Zero shear

We first present the results for 100×100 populations as a function of coupling strength ε for $\Gamma=0$ days^{-1}, i.e., no explicit advection. The results for these simulations have been reported by Guirey *et al.* [20] but are presented here for ease of comparison with the results for nonzero shear ($\Gamma>0$).

TABLE II. Summary of diagnostic statistics.

Measure	Symbol	Range	Units
Phytoplankton biomass of population (i,j)	$P_{i,j}$	0–0.5	gC m^{-3}
Angular frequency of population (i,j)	$\omega_{i,j}$	0.05–0.15	2π $days^{-1}$
Frequency spread	σ	0–25	%
Phase order	R	0–1	
Cluster measures	c_x, c_y	1-n	Grid cells

Figure 1 shows the phytoplankton biomass fields as a function of ε. The emergent spatial structure of the simulation depends in a nonintuitive way on the strength of interaction between populations. The degree of synchrony exhibited by the system does not increase monotonically with coupling strength; there is not a monotonic decrease in σ and increase in R as ε is increased (see Fig. 2). In fact, for ε in the range $0.0025 \leq \varepsilon < 0.02$ $days^{-1}$, there is a coupling-induced desynchronization of populations, indicated by a frequency spread $\sigma \approx 20\%$, an order of magnitude higher than the spread in uncoupled frequencies (Fig. 2). Within this region of apparent disorder, the populations cluster into irregular pockets of locally synchronized dynamics, as seen in Fig. 1. This "patchiness" is temporally evolving but statistically stable, with a characteristic length scale (Fig. 3). The spatial structure of this patchiness is not directly generated by any underlying structure in the parameters of the uncoupled populations, but arises from the interplay between the spatial variability (the spread in phytoplankton growth rates) and dispersal between populations. The cluster measures, c_x and c_y, are equal and increase gradually from around 3 to 7 grid cells as ε is increased within this range, with no effect on σ, which remains at around 20%. For the range of ε leading to clustering of populations, Fig. 4 shows c_x and c_y scaled by the grid-cell length scale $l(\varepsilon)$ to give the size of clusters in km. It is seen that the physical length scale of clusters also varies, *decreasing* from around 50 km to around 20 km over this range of coupling. At $\varepsilon \approx 0.02$ $days^{-1}$, the system undergoes an abrupt switch to frequency-locked, domain-scale dynamics, indicated by $\sigma = 0$ (Fig. 2).

For $\varepsilon \in [0.002, 0.0025]$ $days^{-1}$ and $\varepsilon > 0.02$ $days^{-1}$, the populations are frequency-locked but never fully phase lock; the phase order R gradually approaches but never equals 1 as ε is increased (Fig. 2). The spatiotemporal pattern here is of numerous interfering traveling waves of phase-locked abundance [27,28]. Patches of synchronized biomass are quasiregular, unlike the irregularly shaped clusters seen for $\varepsilon \in [0.001, 0.002)$ $days^{-1}$ and $\varepsilon \in (0.0025, 0.02]$ $days^{-1}$. The spatial scale of these "target patterns" depends on the strength of coupling. The value of ε above which frequency locking persists is referred to as the critical coupling strength for frequency locking, ε_{FL}.

To summarize, the key features of the zero shear case are (i) coupling-induced frequency disorder with small-scale synchronous clustering, (ii) frequency-locked dynamics with larger-scale traveling waves of phase-locked populations and (iii) abrupt bifurcations in emergent spatial dynamics as a function of coupling strength.

B. Shear >0

The phytoplankton biomass fields in gC m^{-3} for $\varepsilon = 0$ $days^{-1}$, $\varepsilon = 0.005$ $days^{-1}$, $\varepsilon = 0.01$ $days^{-1}$, $\varepsilon = 0.02$ $days^{-1}$, $\varepsilon = 0.04$ $days^{-1}$, and $\varepsilon = 0.05$ $days^{-1}$ are shown in Fig. 5 for $\Gamma = 0.001$ $days^{-1}$, $\Gamma = 0.005$ $days^{-1}$, $\Gamma = 0.01$ $days^{-1}$, $\Gamma = 0.05$ $days^{-1}$, and $\Gamma = 0.1$ $days^{-1}$. The biomass plots for $\varepsilon = 0$ all look alike: in the absence of effective diffusivity the plankton populations do not interact and, therefore, do not alter their natural oscillations and are merely advected as a result of the shear, resulting in the same grainy structure of independently oscillating populations for any rate of shear.

Figure 5 clearly shows that under the influence of shear the system exhibits coherent structure (local synchrony or clustering) for a range of effective diffusivity for all rates of shear considered. Figure 6 illustrates the local population dynamics for a desynchronized, clustering case ($\Gamma = 0.01$ $days^{-1}$, $\varepsilon = 0.01$ $days^{-1}$) and a frequency-locked case ($\Gamma = 0.01$ $days^{-1}$, $\varepsilon = 0.04$ $days^{-1}$). Each population retains the basic form of its attractor and is oscillatory for all values of shear and coupling. As for $\Gamma = 0$, small-scale clustering persists for increasing ε until a critical value ε_{FL} at which the whole ensemble frequency-locks and spatial pattern is domain sized.

This is seen more clearly in Fig. 2, which shows the frequency disorder σ and phase coherency parameter R as a function of effective diffusivity for the different rates of shear. The general pattern is as described above for $\Gamma = 0$ and reported by Guirey *et al.* [20], with a region of frequency disorder indicated by high values of σ that increase from $\sigma(\varepsilon = 0) \approx 2.5\%$ to as much as 20%, followed by an abrupt shift to frequency locking signaled by $\sigma \approx 0\%$. For shear rates of $\Gamma = 0.001$, 0.005, 0.01, 0.05 and 0.1 $days^{-1}$, $\varepsilon_{FL} = 0.035$, 0.041, 0.044, 0.027, and 0.019 $days^{-1}$, respectively. However, unlike in the zero shear case, the system "jumps" in and out of frequency locking for values of effective diffusivity lower than the final critical ε_{FL}. This is seen in Fig. 2 as a series of changes in system state from $\sigma \approx 0\%$ to $\sigma \approx 20\%$ and in the biomass plots in Fig. 5 as a succession of transitions from small-scale clustering to domain-scale synchronization and back again as ε is increased. For example, for $\Gamma = 0.001$ $days^{-1}$ Fig. 2 indicates that for $\varepsilon = 0.03$ $days^{-1}$ and $\varepsilon = 0.034$ $days^{-1}$ the system is desynchronized and for $\varepsilon = 0.032$ $days^{-1}$ the system is frequency locked.

Figure 5 shows that, in comparison with the zero shear case, the inclusion of shear alters the spatial characteristics of the clustering seen in the ranges $0 < \varepsilon < \varepsilon_{FL}$. The advection

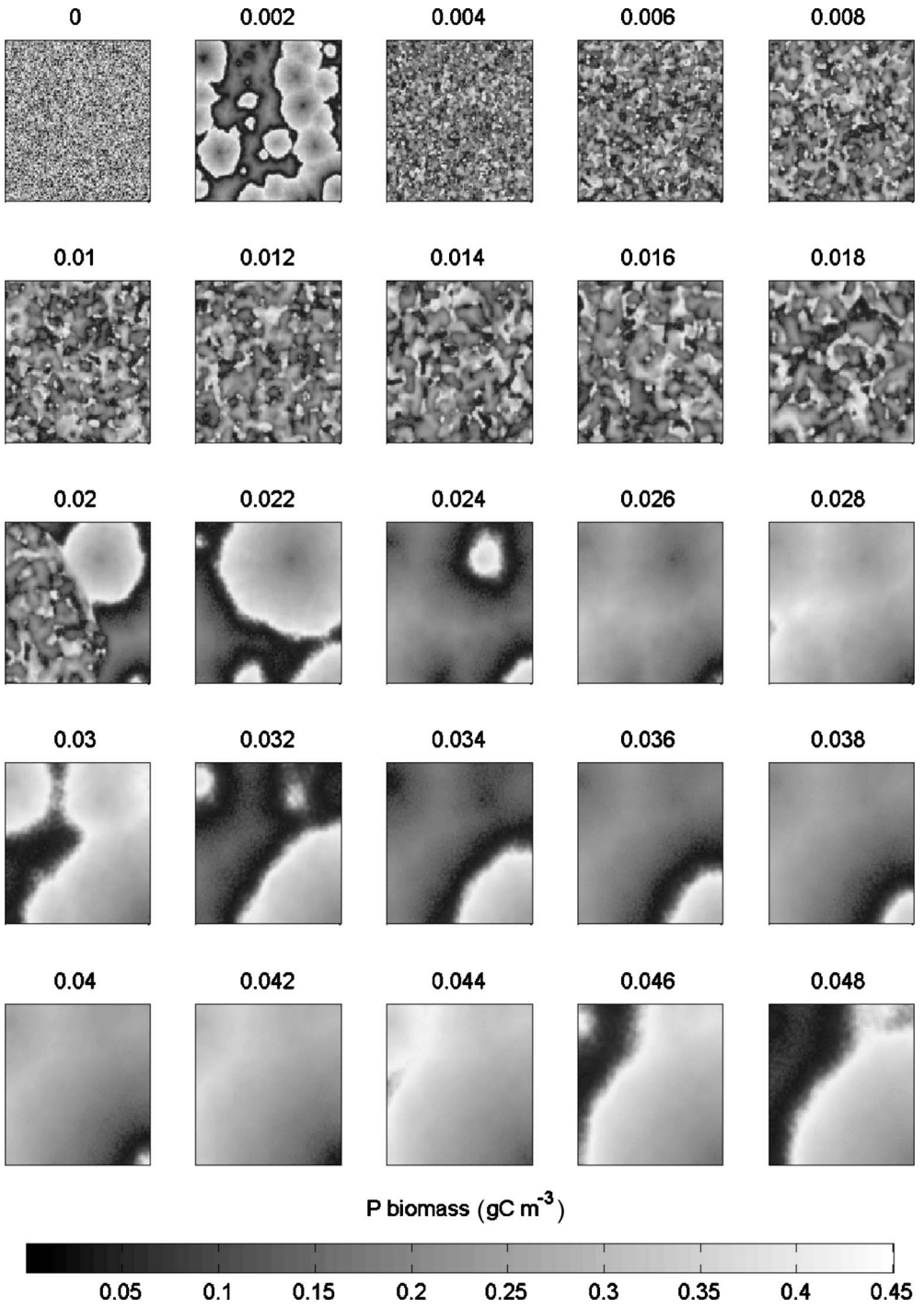

FIG. 1. Zero shear. Phytoplankton biomass in gC m^{-3} for 100×100 populations as a function of nearest-neighbor coupling strength ε for $\Gamma = 0$. Simulations were run until diagnostics reached steady state (see text). Subplot labels indicate the value of ε in $days^{-1}$.

does not destroy the local synchrony; there is still clear evidence of coherent structure. Even for the largest shear ($\Gamma = 0.1$ $days^{-1}$), the clusters are not simply stripes of uniform phytoplankton biomass aligned with the x direction, as might be expected. This indicates that the spatial positioning of the clusters is nonstationary, since otherwise the effect of shear would be to narrow and stretch the clusters until they reached a steady state as a horizontal stripe. The populations composing each "patch" vary in time.

For the lowest values of shear, $\Gamma = 0.001$ $days^{-1}$ and $\Gamma = 0.005$ $days^{-1}$, the clustering observed in Fig. 5 is indistinguishable by eye from the kind of structure seen in the zero shear case in Fig. 1. The shear rate is too slow to impose directionality upon the clustering generated by the effectively diffusive coupling. For higher values of shear, $\Gamma = 0.01$ $days^{-1}$, $\Gamma = 0.05$ $days^{-1}$, and $\Gamma = 0.1$ $days^{-1}$, there is a definite directionality to the spatial structure. With respect to the no-shear simulation, the clusters are narrowed and

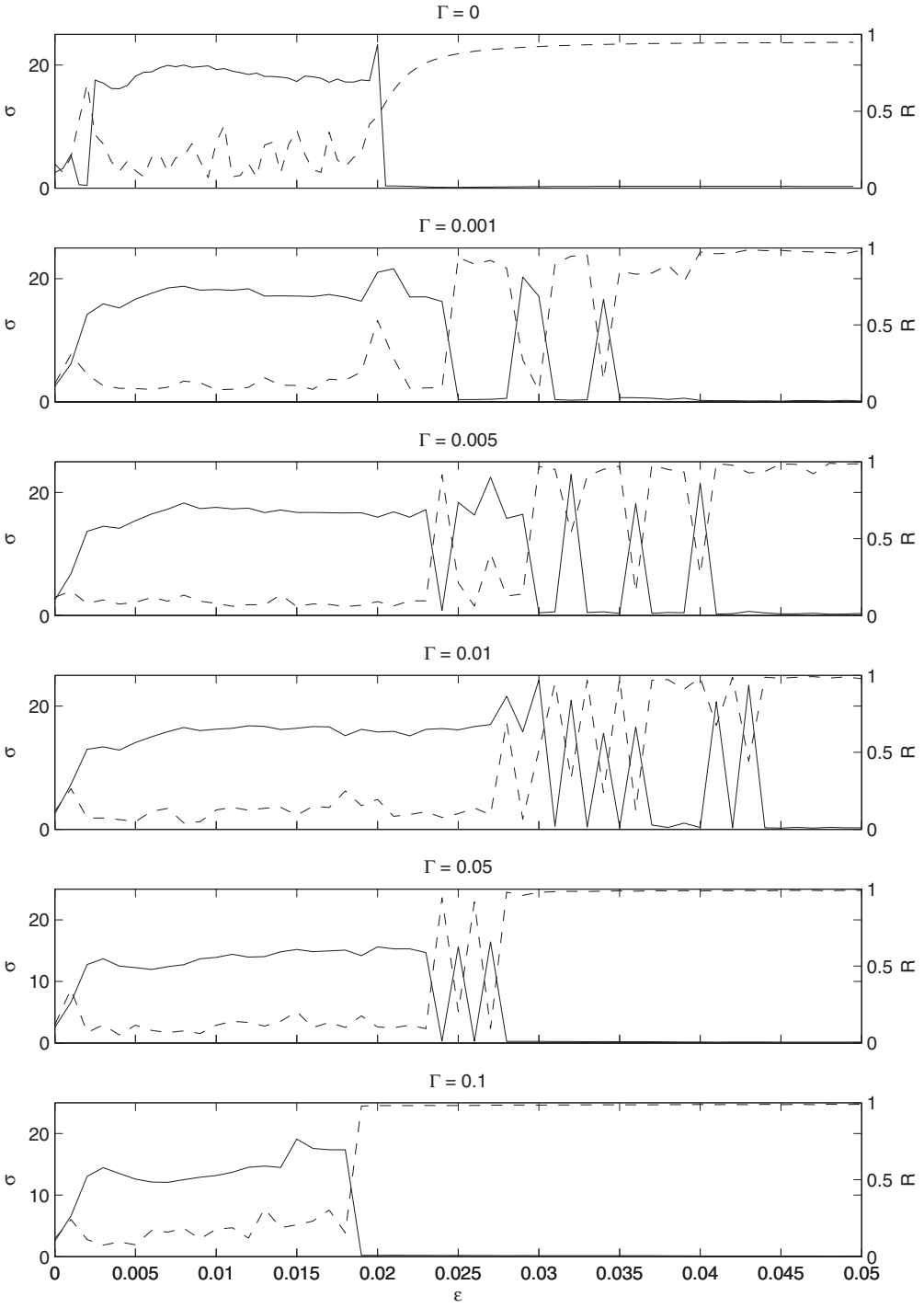

FIG. 2. Synchronization diagnostics. Frequency spread σ and phase order R for 100×100 populations as a function of nearest-neighbor coupling strength ε and shear Γ. Subplot headings give Γ in days^{-1}.

stretched by the shear and are increasingly aligned with the x axis, but are still nonstationary.

The change in structure that can be seen by eye is well supported by the cluster measures $c_x(\varepsilon)$ and $c_y(\varepsilon)$ shown in Fig. 3. The cluster measure only has clear meaning outside the frequency-locked regions (see Guirey *et al.* [20]). Hence we only discuss the behavior of the cluster measures in the desynchronized region, i.e., where small-scale clustering dominates.

For $\Gamma=0.001$ days^{-1} and $\Gamma=0.005$ days^{-1}, $c_x(\varepsilon)\approx c_y(\varepsilon)$ for all $\varepsilon<\varepsilon_{\mathrm{FL}}$, confirming that the clusters are not skewed in a particular direction. There is a steady increase in c_x and c_y from 1 to 8 grid cells with increasing ε, interrupted by the aforementioned "jumps" to the frequency locked state. For $\Gamma=0.01$ days^{-1}, $c_x(\varepsilon)>c_y(\varepsilon)\forall\ \varepsilon<\varepsilon_{\mathrm{FL}}$, with c_x increasing from 1 to 10 grid cells and c_y increasing from 1 to 8 grid cells with increasing ε. The difference $|c_x-c_y|$ between the cluster size in each direction increases with increasing ε. The

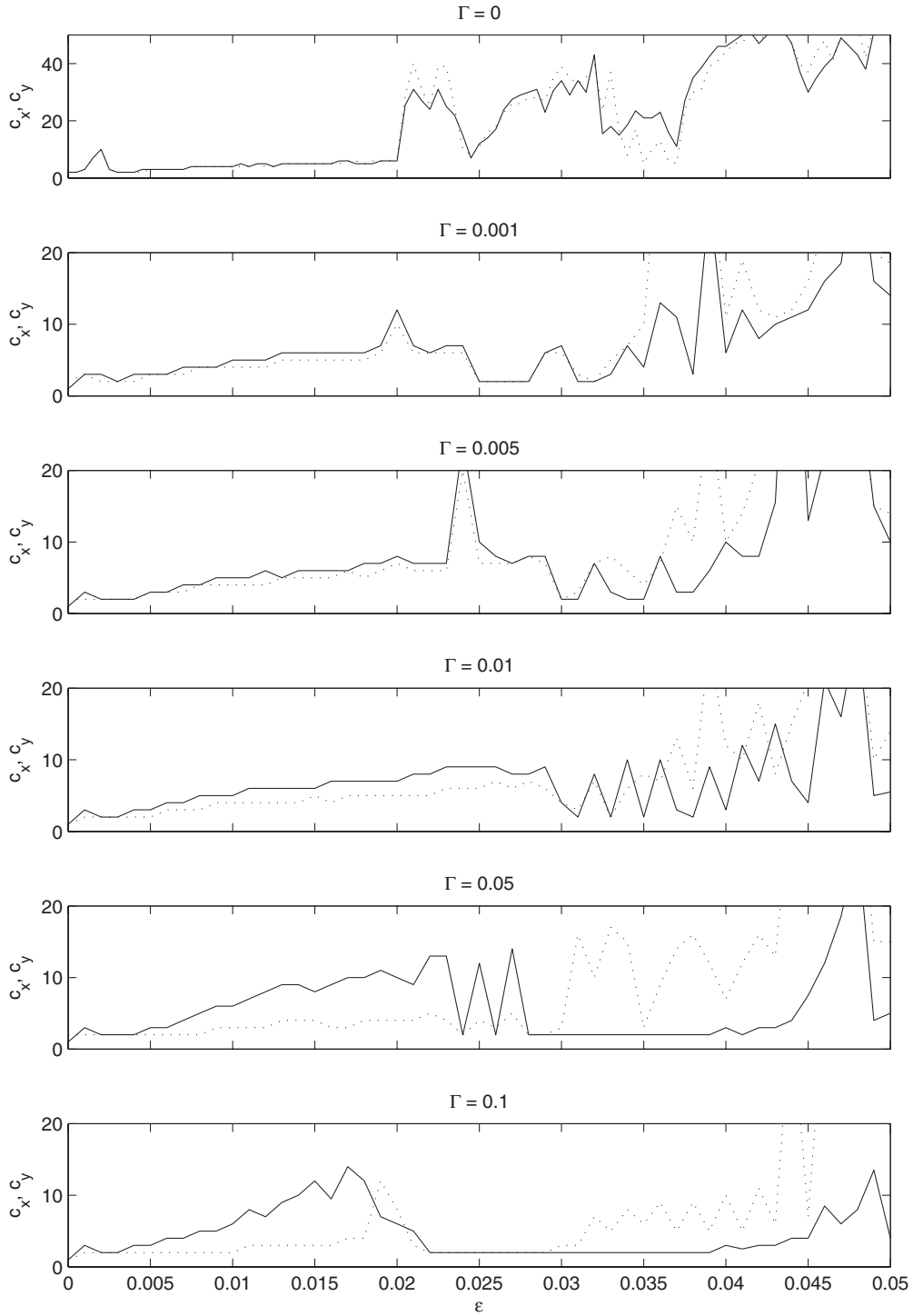

FIG. 3. Spatial diagnostics (grid cells). Cluster measures c_x (solid) and c_y (dotted) in numbers of grid-cells for 100×100 populations as a function of nearest-neighbor coupling strength ε and shear Γ. Subplot headings give Γ in days^{-1}.

same trend is seen more markedly for increasing shear. For $\Gamma = 0.05$ days^{-1}, c_x increases from 1 to 14 grid cells, whilst c_y increases from 1 to only 5 grid-cells, and for $\Gamma = 0.1$ days^{-1}, c_x increases from 1 to 15 grid cells, whilst c_y increases from 1 to only 4 grid cells with increasing ε. These numbers show a trend of increasing stretching of clusters in the x direction and narrowing in the y direction, as expected from the shear applied to the ensemble. Over the clustering region of ε, Fig. 4 shows that the physical scale of spatial structure in km is also not constant; there is a trend of decreasing length scale of clustering with increasing ε.

In all cases, for $\varepsilon > \varepsilon_{\mathrm{FL}}$ the order parameter R tends rapidly to 1 (see Fig. 2). As observed for zero shear, quasiregular traveling waves occur (e.g., for $\Gamma = 0.001$ days^{-1} and $\varepsilon = 0.02$ days^{-1}; see Fig. 5). However, the waves are less distinct, showing less variation in abundance, because the system is closer to phase locking. For high shear (e.g., for $\Gamma = 0.1$ days^{-1} and $\varepsilon = 0.02$ days^{-1}; see Fig. 5), the regions of

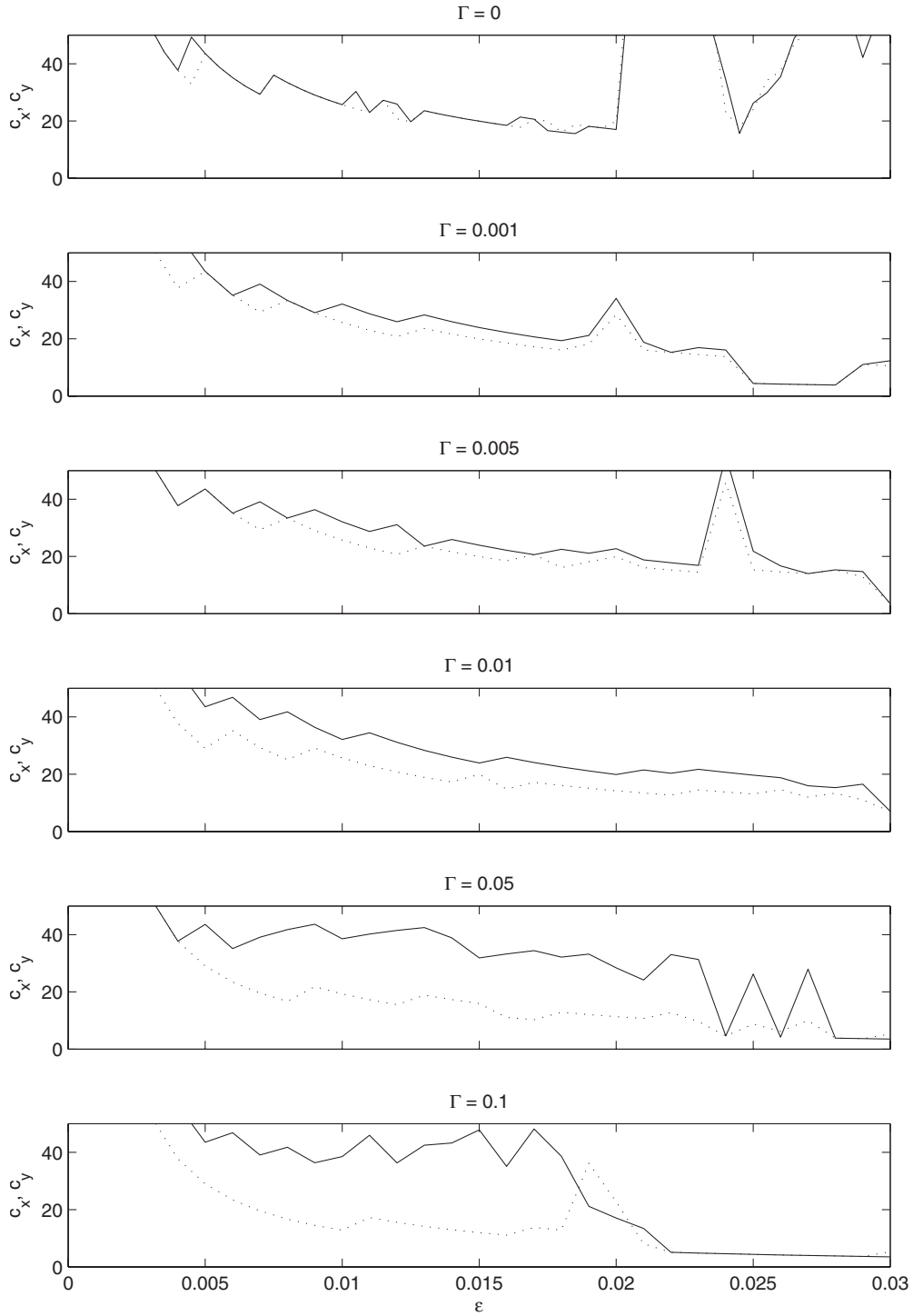

FIG. 4. Spatial diagnostics (km). Cluster measures c_x (solid) and c_y (dotted) in km for 100×100 populations as a function of nearest-neighbor coupling strength ε and shear Γ. Focus is on the range of ε for which frequency disorder and spatial clustering occur. Subplot headings give Γ in days^{-1}.

phase-locked abundance are stretched by the flow, as described above, instead of occurring as quasiregular waves.

There is no clear pattern in the value of $\varepsilon_{\mathrm{FL}}$ with increasing Γ. However, it is evident that the inclusion of realistic levels of shear alters the spatial characteristics of the ensemble whilst allowing coherent clusters to persist.

C. Influence of subpopulation natural properties

Figure 7 shows the calculations of σ as a function of ε for each of the spatial configurations of the set $\{a_{i,j}\}$ that are possible under the influence of the shear for $\Gamma=0$ days^{-1}, $\Gamma=0.001$ days^{-1}, and $\Gamma=0.1$ days^{-1} for 10×10 populations. To clarify, each simulation uses the same set of phytoplank-

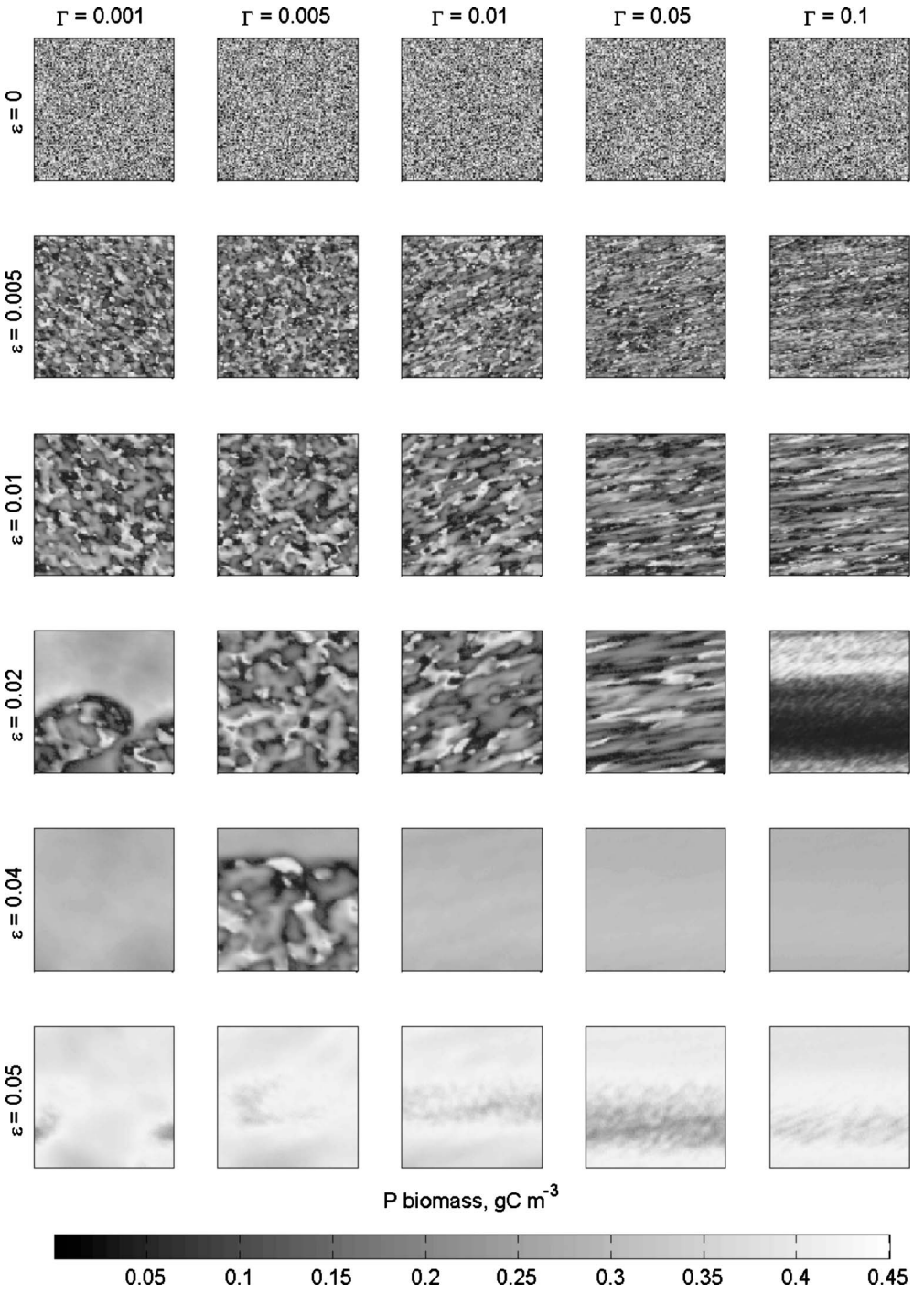

FIG. 5. Shear ≥ 0. Phytoplankton biomass in gC m^{-3} for 100×100 populations as a function of nearest-neighbor coupling strength ε and shear Γ. Simulations were run until diagnostics reached steady state (see text). Row labels indicate the value of ε in $days^{-1}$; column labels indicate Γ in $days^{-1}$.

ton growth rates but in a different spatial configuration. Ten different configurations with grid cells aligned are possible under this advection scheme.

For $\Gamma=0$ $days^{-1}$, the initial arrangement of natural frequencies is constant with time. The resultant ε_{FL} is seen to range from $\min(\varepsilon_{FL})=0.002$ $days^{-1}$ to $\max(\varepsilon_{FL})=0.016$ $days^{-1}$, each spatial arrangement leading to a specific ε_{FL} (Fig. 7). For nonzero shear, the initially imposed spatial arrangement of natural frequencies varies with time, at a rate dependent upon Γ.

For $\Gamma=0.001$ $days^{-1}$, for each initial configuration of populations, there is a range of ε for which the ensemble dynamics move in and out of frequency locking with increasing ε before eventually permanently frequency locking. This range is roughly coincident with the range of $\varepsilon_{FL} \in [0.002, 0.016]$ $days^{-1}$ found above for $\Gamma=0$ $days^{-1}$. For

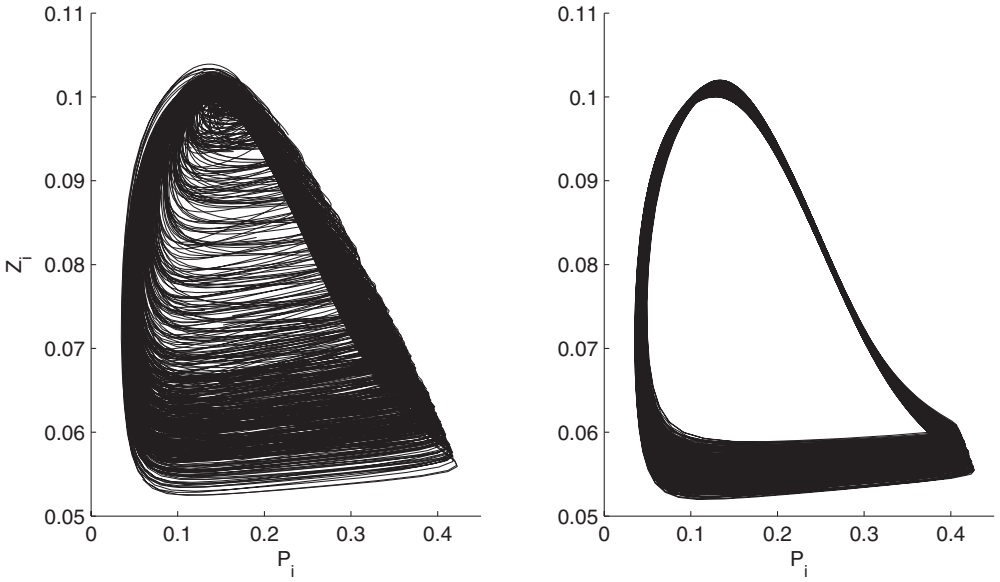

FIG. 6. State space $(P_{i,j},Z_{i,j})$ for all populations for an example desynchronized, clustering case (left; $\Gamma=0.01$ days^{-1}, $\varepsilon=0.01$ days^{-1}) and a frequency-locked case (right; $\Gamma=0.01$ days^{-1}, $\varepsilon=0.04$ days^{-1}).

$\Gamma=0.1$ days^{-1} the ensemble is frequency locked for $\varepsilon > 0.002$ days^{-1} and the profile of σ with varying ε looks alike for all initial spatial configurations of the populations (see Fig. 7).

These results show that the impact of the time-dependent spatial arrangement of subpopulations on the ability of the system to synchronize depends on the rate of shear. The rearrangement of populations, and corresponding natural frequencies, with time leads to a time-dependent value of critical coupling and causes a succession of transitions within this range. For low shear ($\Gamma=0.001$ days^{-1}), the time scale of the advection is $T_\Gamma=\frac{1}{\Gamma}=1000$ days, which, within the range of effective diffusivities $\varepsilon \in [0.002, 0.016]$ days^{-1}, gives $T_\Gamma > T_\varepsilon$. Hence, the dominant effect on the ensemble dynamics is the effective diffusivity, with the system being pulled towards frequency locking at a value of ε varying with the time-dependent configuration of populations. This is what causes the "jumping" between the frequency-locked and disordered states described in the previous section (Figs. 5, 2, and 3). For $\Gamma=0.1$ days^{-1}, we have $T_\Gamma=10$ days, so that $T_\Gamma < T_\varepsilon$ for the full range of effective diffusivity. In this case, the faster shear actually alters the ability of the ensemble to synchronize, by increasing the network of influence of each population. In other words, advection at this rate allows each population to be coupled with a greater number of populations on the relevant time scale and, therefore, effectively alters the coupling geometry of the system and enhances the subgrid mixing. Hence, advection increases the ability of the lattice of populations to synchronize their dynamics.

IV. DISCUSSION AND CONCLUSIONS

In this study, we have incorporated an explicit advection scheme into a standard model for spatially extended plankon dynamics. The rate of shear has been varied in order to investigate how the emergent spatiotemporal dynamics of the simulation are modified by explicit advection. The primary aim has been to establish whether the results and methods of synchronization theory from terrestrial population dynamics and previous work on spatial structure in plankton dynamics are relevant in a marine context. In particular, we asked whether the inclusion of explicit stirring would prevent formation of coherent structure created by synchronous clustering of populations.

It has been found that many of the features seen for the mixing-only simulation also occur under the action of advection. The properties of synchrony exhibited by the system as a function of the coupling strength are broadly similar, with an "anomalous region" of increased frequency disorder and small-scale clustering followed by a shift to frequency locking at a critical coupling strength $\varepsilon_{\mathrm{FL}}$. For nonzero shear, there is not a single value of ε at which the transition to frequency locking occurs; rather, the system moves in and out of frequency locking as a function of ε until eventually remaining frequency-locked for coupling higher than the critical value.

We have shown that this "jumping" results from the time-varying spatial arrangement of the populations caused by advection; $\varepsilon_{\mathrm{FL}}$ varies with the spatial arrangement of natural frequencies and hence is time varying, potentially resulting in transitions in and out of frequency locking. The impact of the spatial arrangement of natural frequencies on the synchronization of coupling oscillators has been seen previously by Osipov and Sushchik [23].

This phenomenon is dependent on the rate of shear. For the fastest shear ($\Gamma=0.1$ days^{-1}), there is only one transition to frequency locking, as in the mixing-only ($\Gamma=0$) case. This is because the time scale of advection (10 days) is faster than that of the biological dynamics ($\sim$100 days) and the effective diffusivity ($>$50 days). The rapid rearrangement of populations allows previously separated populations to interact on time scales faster than the other influences on the

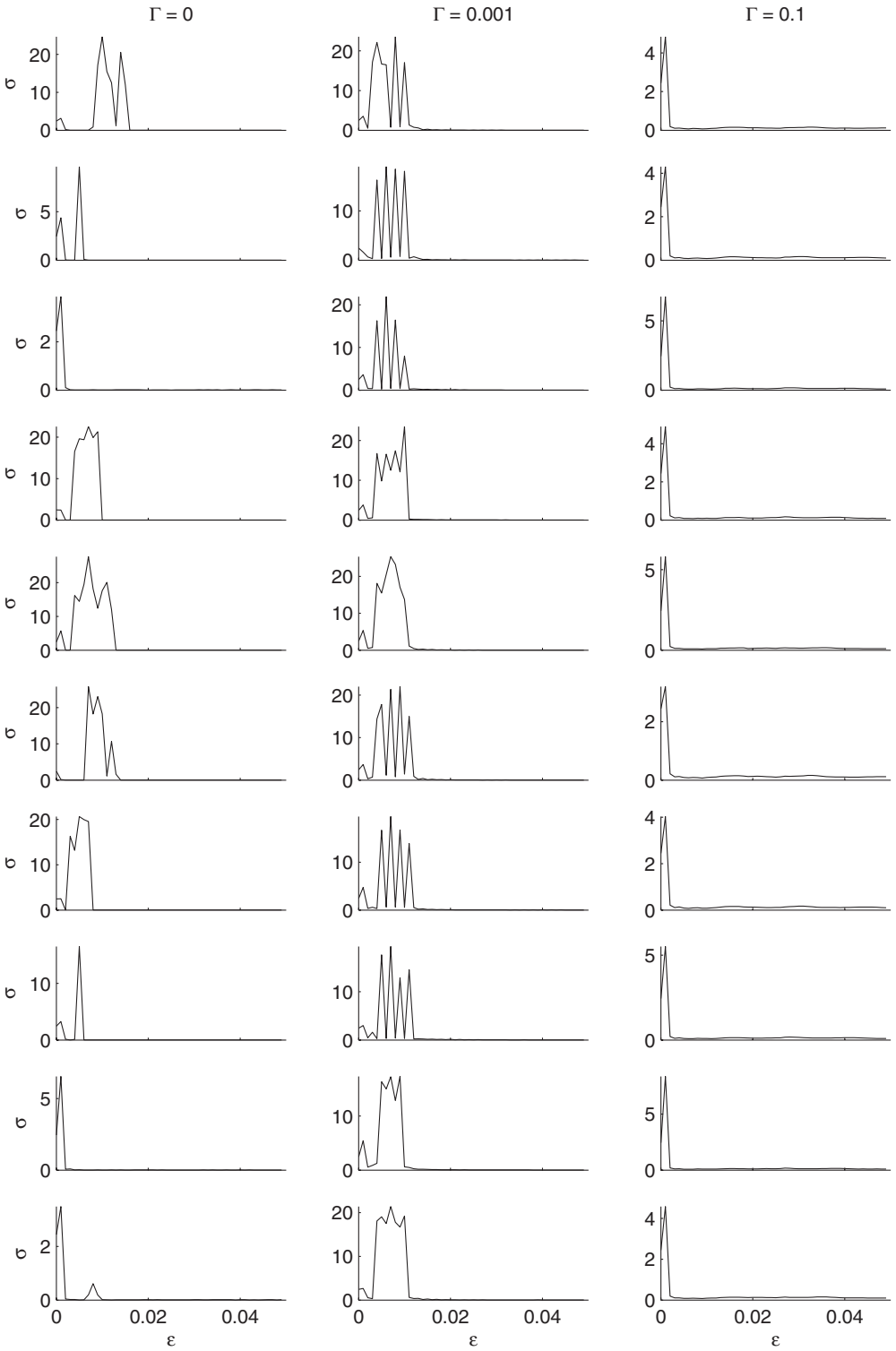

FIG. 7. Impact of spatial arrangement of populations. Frequency spread σ as a function of nearest-neighbor coupling strength ε for 10×10 populations for shear $\Gamma=0$, 0.001 and 0.1 days^{-1}. The nonidentical subpopulations, with population-specific phytoplankton growth rate, are initialized in each of the ten spatial arrangements possible under the influence of the shear; each row of subplots gives the results for one spatial arrangement.

dynamics. The net effect is to effectively alter the coupling geometry of the system, increasing the range of influence of each population and reducing the variability in $\varepsilon_{\mathrm{FL}}$ associated with the spatial arrangement of natural frequencies. This does not occur for slower advection because the time scale of interaction of separated populations is longer than that of the nearest-neighbor coupling. Modification of the coupling geometry of a system by explicit stirring has been reported by Neufeld [39]. A more realistic representation of upper ocean stirring and mixing could allow populations to come into

contact with a larger number of populations in the simulation. Clearly the particular spatial arrangement of natural frequencies would then be less influential.

With the inclusion of advection, the bifurcations in system-level dynamics reported by previous authors [17–20] still occur. The emergent spatial structure of a simulation may alter from patchy to homogenous as an apparently innocuous model parameter is varied. For example, it has been seen here that system-level dynamics may be frequency locked with large-scale structure or desynchronized with small-scale clustering even though domain size, spatial resolution, number of populations, parameter spread, biological model and coupling strength are all fixed and only the particular spatial arrangement of population parameters, with a standard deviation of only 5%, is varied. Further work (see Appendix) explored this sensitivity further by varying the phytoplankton growth rate values, taking them from the same uniform distribution but varying the seed value used in the random number generator. No shear was applied, so that the spatial arrangements of natural frequencies remained constant in time. $\sigma(\varepsilon)$ was calculated for each set of growth rates. It was found that the ability of the coupled populations to synchronize their dynamics varied enormously. The frequency-disorder region did not always occur and its occurrence or otherwise was not related to the natural frequency spread, $\sigma(\varepsilon=0)$. This result is of concern to biophysical modelers wishing to objectively investigate plankton patchiness and its biogeochemical consequences in their models. This alarming sensitivity to the spatial arrangement of natural frequencies appears to be mitigated by sufficiently fast stirring. Further work should also investigate the sensitivity to the width and probability distribution of mismatch in the biological model parameters, and should relate this to observed patterns of variability in biological measurements in the ocean.

The results from this study suggest that explicit advection increases the ability of coupled plankton populations to synchronize their dynamics. First, for coupling strengths greater than the critical value for frequency locking, the simulations phase-lock almost instantly for non-zero shear; in the case of zero shear, the approach to phase locking is slow and gradual and the simulation never fully phase locks for the full range of nearest neighbor coupling. Second, all simulations found that the fastest rate of shear resulted in the lowest value of critical coupling for frequency locking. However, no clear relationship was found between the rate of shear and the critical coupling strength. This is because of the confounding influence of the variability in $\varepsilon_{\mathrm{FL}}$ caused by the time-varying arrangement of population natural properties. To remove this effect, further work could look at not allowing the populations to advect with the parcels of water, i.e., making the assumption that the spatial variability in biological parameters is (indirectly) related to spatially fixed properties such as bathymetry. Here, it was chosen to focus on the more oceanographically relevant case of advection with the water parcels.

Most importantly, we have seen that for realistic rates of surface ocean shear, the spatial clustering of populations into subsets of locally synchronized dynamics, as reported in the case of no explicit advection, still occurs; the inclusion of stirring does not prevent the formation of spatial structure. Exclusion of explicit stirring from previous work on synchronization in spatial plankton distributions raised the question of how applicable the results would be to the marine environment. The results presented here move the approach away from terrestrial metapopulation dynamics and provide support for the use of synchronization theory methods and results in exploring spatial structure in surface ocean biophysical simulations.

Inclusion of stirring alters the characteristics of the spatial structure. Advection draws the clusters out in the direction of the flow, causing stretching and narrowing of the patches of synchronized dynamics. This stretching and narrowing is the mechanism responsible for the filamental structure observed in real-world plankton distributions observed by satellite (e.g., [40]) and from research ships [38]. We have seen that the degree of elongation and narrowing of clusters depends on the rate of shear. Even for the largest shear, the clusters are not simply stripes of uniform biomass aligned with the flow. This indicates that the spatial positioning of the clusters is nonstationary, since otherwise the effect would be to narrow and stretch the clusters until they reached a steady state as a horizontal stripe.

In conclusion, these results have shown that explicit stirring does not prevent the formation of coherent structure in biophysical simulations through the clustering of populations into patches of synchronized dynamics. This affirms the applicability of synchronization theory in the study of plankton patchiness. By incorporating many features of typical ocean situations, in a framework simple enough to allow analysis of the relative influences on the biological dynamics of a spatial plankton distribution, this work provides the basis for future studies incorporating a more realistic ocean flow.

ACKNOWLEDGMENTS

E.J.G. is grateful for an Environmental Mathematics and Statistics Programme Research Studentship jointly funded by NERC and EPSRC. This paper forms part of the contribution by the National Oceanography Centre, Southampton, (MAS and APM) to Theme 2 of the Oceans 2025 programme funded by NERC. MAB acknowledges EPSRC funding Grant No. EP/D073398/1. We acknowledge the lasting influence of Professor Mike Fasham FRS, whose work on oceanic ecosystem modelling was the original inspiration for our studies. The authors thank two anonymous reviewers whose comments helped to improve the paper.

APPENDIX

This section presents experiments that were carried out to further investigate the finding that the spatial arrangement of nonidentical populations has a strong influence on the ability of the coupled populations to synchronize their dynamics (see Results).

100 simulations were carried out of a lattice of 10×10 populations. The populations interact via the nearest neighbor coupling of strength ε but there is no shear. The biological dynamics are represented by the NPZ model described

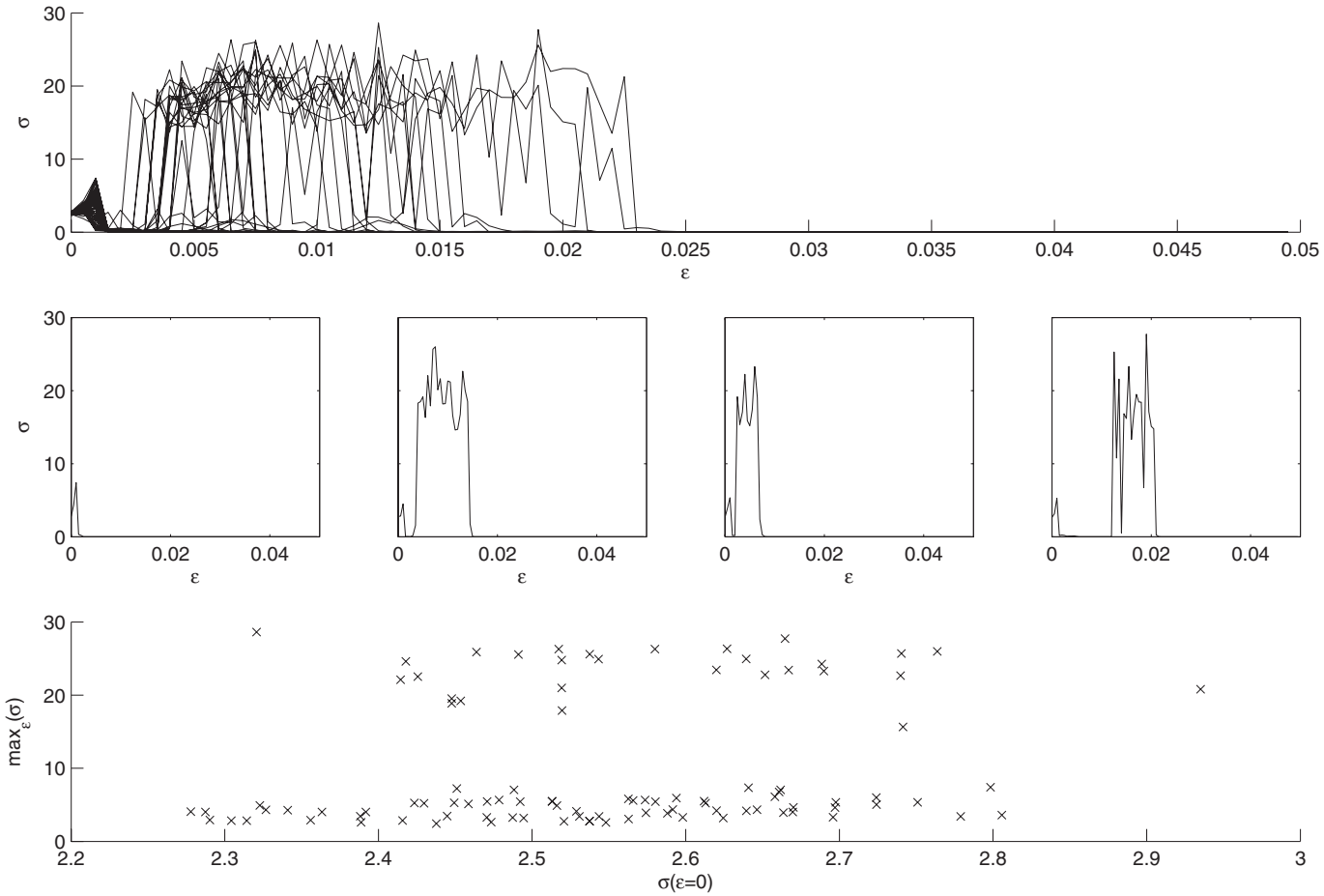

FIG. 8. Impact of population natural frequencies. Results of varying the set of phytoplankton growth rates $a_{i,j}$ for a 100 runs of 10 $\times$ 10 populations for zero shear. For each simulation, a different integer seed is used in the generation of random mismatch values from the same uniform distribution. Top panel shows the frequency spread σ as a function of nearest neighbor coupling strength ε for all 100 runs. Middle panel shows four characteristic examples. Bottom panel shows the maximum against the natural spread in frequencies.

above. For each simulation, the set of phytoplankton growth rates $a_{i,j}$ is chosen from the same uniform distribution of width $\Delta=5\%$ but using a different integer seed for the random number generator. A different seed leads to a different set of random numbers. Therefore, each simulation varies only in the particular values of $a_{i,j}$ taken from the same probability distribution. Because the rate of shear is zero, the spatial arrangement of populations is constant in time. Each simulation is run until the diagnostics described in the Methods are at steady state.

Figure 8 shows the calculation of the frequency spread σ of populations as a function of ε for each simulation (top panel) and gives four characteristic examples (middle panel). There is huge variability in the curve $\sigma(\varepsilon)$. All simulations are alike for $\epsilon \leq 0.002$, with a small increase in frequency spread followed by a transition to frequency locking, although the maximum frequency spread attained in this region varies between simulations. For $\epsilon > 0.002$, the simulations fall into two categories. Either, the simulation bursts out of frequency locking, entering a region of high frequency disorder before returning to frequency locking at a value $\varepsilon_{\mathrm{FL}}$ that varies with simulation; or, the frequency-disorder region does not occur and the system remains frequency locked. The third panel of Fig. 8 shows a scatter plot of the maximum frequency spread attained over the range of ε against the natural (uncoupled) frequency spread. The two distinct behaviors can be seen in the scatter plot as two clouds of points with $\max_{\varepsilon}(\sigma) \approx 25\%$ and $\max_{\varepsilon}(\sigma) \approx 5\%$, respectively. It might be supposed that the maximum frequency spread, and the occurrence or otherwise of a frequency-disorder region, would be related to the natural frequency spread. Figure 8 shows that this is not the case. The natural frequency spread varies from 2.3% to 2.9% and there is no relationship with the maximum frequency spread. This shows that the spatial arrangement of the natural frequencies is important.

[1] A. Pikovsky, M. Rosenblum, and J. Kurths, *Synchronization: A Universal Concept in Nonlinear Sciences* (Cambridge University Press, Cambridge, England, 2001).
[2] S. Taherion and Y.-C. Lai, Phys. Rev. E **59**, R6247 (1999).
[3] J. Neff and T. L. Carroll, Sci. Am. **296**, 101 (1993).
[4] S. Barbay, G. Giacomelli, and F. Marin, Phys. Rev. E **61**, 157 (2000).
[5] L. Stone, R. Olinky, B. Blasius, A. Huppert, and B. Cazelles, AIP Conf. Proc. **622**, 476 (2002).
[6] J. Buck and E. Buck, Science **159**, 1319 (1968).
[7] M. K. McClintock, Nature (London) **229**, 244 (1971).
[8] Z. Néda, E. Ravasz, Y. Brechet, T. Vicsek, and A. L. Barabási, Nature (London) **403**, 849 (2000).
[9] T. N. Sherratt, X. Lambin, S. J. Petty, J. L. Mackinnon, C. F. Coles, and C. J. Thomas, J. Appl. Ecol. **37**, 148 (2000).
[10] R. C. Ydenberg, Oikos **50**, 270 (1987).
[11] D. T. Haydon, N. C. Stenseth, M. S. Boyce, and P. E. Greenwood, Ecology **98**, 13149 (2001).
[12] E. Ranta, V. Kaitala, J. Lindstrom, and H. Linden, Proc. R. Soc. London, Ser. B **262**, 113 (1995).
[13] B. T. Grenfall, K. Wilson, B. F. Finkenstädt, T. N. Coulson, S. Murray, S. D. Albon, J. M. Pemberton, T. H. Clutton-Brock, and M. J. Crawley, Nature (London) **394**, 674 (1998).
[14] T. G. Benton, C. T. Lapsley, and A. P. Beckerman, Ecol. Lett. **4**, 236 (2001).
[15] D. A. Vasseur and J. W. Fox, Nature (London) **460**, 1007 (2009).
[16] B. Blasius, E. Montbrió, and J. Kurths, Phys. Rev. E **67**, 035204(R) (2003).
[17] R. M. Hillary and M. A. Bees, Phys. Rev. E **69**, 031913 (2004).
[18] R. M. Hillary and M. A. Bees, Bull. Math. Biol. **66**, 1909 (2004).
[19] E. J. Guirey, M. A. Bees, A. P. Martin, M. A. Srokosz, and M. J. R. Fasham, Bull. Math. Biol. **69**, 1401 (2007).
[20] E. J. Guirey, A. P. Martin, M. A. Srokosz, and M. A. Bees, Ocean Modelling **29**, 223 (2009).
[21] M. Holyoak and S. P. Lawler, Ecology **77**, 1867 (1996).
[22] C. Elton and M. Nicholson, J. Anim. Ecol. **11**, 215 (1942).
[23] G. V. Osipov and M. M. Sushchik, IEEE Trans. Circuits Syst., I: Fundam. Theory Appl. **44**, 1006 (1997).
[24] I. Belykh, V. Belykh, K. Nevidin, and M. Hasler, Chaos **13**, 165 (2003).
[25] M. Pascual, M. Roy, F. Guichard, and G. Flierl, Philos. Trans. R. Soc. London, Ser. B **357**, 657 (2002).
[26] F. D. Smet and D. Aeyels, Proc. R. Soc. London, Ser. A **465**, 745 (2009).
[27] B. Blasius, A. Huppert, and L. Stone, Nature (London) **399**, 354 (1999).
[28] B. Blasius and R. Tönjes, Phys. Rev. Lett. **95**, 084101 (2005).
[29] A. P. Martin, Prog. Oceanogr. **57**, 125 (2003).
[30] J. H. Steele and E. W. Henderson, Am. Nat. **344**, 734 (1981).
[31] A. M. Edwards and J. Brindley, Dyn. Stab. Syst. **11**, 347 (1996).
[32] A. M. Edwards and J. Brindley, Bull. Math. Biol. **61**, 303 (1999).
[33] R. W. Eppley, Fish. Bull. **70**, 1063 (1972).
[34] A. E. Alpine and J. E. Cloern, Mar. Ecol.: Prog. Ser. **44**, 167 (1988).
[35] A. Okubo, Deep-Sea Res. **18**, 789 (1971).
[36] H. Fujisaka and T. Yamada, Prog. Theor. Phys. **69**, 32 (1983).
[37] M. A. Sundermeyer and J. F. Price, J. Geophys. Res. **103**, 21481 (1998).
[38] E. Abraham, C. S. Law, P. W. Boyd, S. J. Lavendar, M. T. Maldonado, and A. R. Bowie, Nature (London) **407**, 727 (2000).
[39] Z. Neufeld, I. Z. Kiss, C. Zhou, and J. Kurths, Phys. Rev. Lett. **91**, 084101 (2003).
[40] F. d'Ovido, J. Isern-Fontanet, C. Lòpez, E. Hernàndez-Garcìa, and E. Garcìa-Ladona, Deep-Sea Res., Part I **56**, 15 (2009).